

# Experimental Evaluation of RSA Algorithms for SDN-programmable VCSEL-based S-BVT in High-Capacity and Cost-Efficient Optical Metro Networks

R. Martínez<sup>1</sup>, R. Casellas<sup>1</sup>, M. Svaluto Moreolo<sup>1</sup>, J. M. Fabrega<sup>1</sup>, R. Vilalta<sup>1</sup>,  
R. Muñoz<sup>1</sup>, L. Nadal<sup>1</sup>, J. P. Fernández Palacios<sup>2</sup>, V. López<sup>2</sup>, D. Larrabeiti<sup>3</sup> and  
G. Otero<sup>3</sup>

<sup>1</sup> Centre Tecnològic de Telecomunicacions de Catalunya (CERCA/CTTC), Castelldefels, Spain

<sup>2</sup> Telefónica I+D, GTCO, Madrid, Spain

<sup>3</sup> Universidad Carlos III, Madrid, Spain  
ricardo.martinez@cttc.es

**Abstract.** Future metro networks need to increase the transport capacity and improve the cost- and power-efficiency. These challenges are tackled by the EU-H2020 PASSION project exploiting dense photonic integration and cost-efficient optical technologies. Specifically, PASSION investigates a) modular sliceable bandwidth variable transceivers (S-BVTs) built upon a set of both vertical cavity surface emitting lasers (VCSEL) and Coherent Receivers (CO-Rx); and b) hierarchical switching nodes in a flexigrid network. An SDN controller handles the network programmability where a key functionality is the path computation and resource selection to fulfil the connection requirements. This is conducted by the Routing and Spectrum Assignment (RSA) algorithms. The considered S-BVT transmitter imposes that each S-BVT VCSEL reaches up to 50 Gb/s. Thus, connections requesting higher bandwidth (e.g., 200 Gb/s) are accommodated over several optical flows. In this context, two RSA algorithms called *co-routed* (RSA-CR) and *inversed multiplexed* (RSA-IM) optical flows are proposed and compared. The RSA-CR enforces that all the connection's optical flows are routed over the same spatial path; the RSA-IM relaxes this allowing the optical flows being set up over different spatial routes. The experimental evaluation, made upon dynamic traffic, aims at comparing both RSA algorithms performance according to the blocked bandwidth ratio, the average used of S-BVT devices, and the average setup time.

**Keywords:** SDN, Flexi-Grid Metro Networks, S-BVT.

## 1 Introduction

The design of the metro networks is becoming crucial to deal with the requirements bound to the 5G services with respect to both huge transport capacity and very high dynamicity. In this context, as discussed in [1], 33% of the total transport capacity offered by the telecom operators will strictly remain within the metro networks. Thereby,

such network segments need to be enhanced to support not only fully programable infrastructure, but also efficiently designed to lower operational and capital expenditures (e.g., cost, energy consumption, etc.) [2]. These challenges are being investigated within the EU H2020 PASSION project [5]. PASSION project aims at exploiting the advantages of programmable and photonic technologies over flexigrid networks [3] such as optical transceivers.

The automatic network configuration is attained by a centralized Software-Defined Networking (SDN) controller. This controller uses defined control interfaces (APIs) to interact with the control agents locally handling the programmability of every underlying network element and/or devices (i.e., optical switch and transceivers). To offer high transport capacity (i.e., Tb/s) at low cost and power within the metro networks, the PASSION project defines and deploys a modular sliceable bandwidth transceiver (S-BVT). This S-BVT leverages new appealing photonic technologies such as the vertical cavity surface emitting laser (VCSEL) at long wavelengths [4]. Moreover, the targeted metro network is formed by heterogeneous optical switches providing both the transport as well as the aggregation functions of the optical flows. These optical switches are associated to a so-called Hierarchical Level (HL). As described in [5], four HLs are considered, namely: HL4, HL3 and HL2/1. Each of them defines specific switch characteristics such as the capability of either originate/terminate optical flows (i.e., add/drop operations) or enabling optical bypassing. In brief, HL4 and HL2/1 nodes border the access and core network segments, respectively; HL3 nodes are the transit optical switches interconnecting both HL4 and HL2/1 nodes. In this work, optical connections are always set up from HL4 to HL2/1 (an vice versa) traversing HL3 switches.

In the PASSION-designed S-BVTs, each constituting VCSEL element has a 20 GHz-bandwidth providing up to 50 Gb/s ( $r^{VCSEL}$ ). Optical connections requests ( $req$ ) may demand larger bandwidth ( $b$ ) than  $r^{VCSEL}$ , e.g., 100, 200, or 400 Gb/s. This entails to allocate  $N$  ( $\geq 1$ ) VCSELs (operating at different wavelengths) at the corresponding ingress S-BVT device to accommodate a  $req$ . Consequently,  $N$  different optical flows may need to be set up between the ingress and egress nodes. As an example, a  $req$  demanding 200 Gb/s requires allocating 4 different VCSELs at the ingress node, 4 Co-Rxs at the egress node, and 4 optical flows over the route interconnecting the ingress and the egress nodes. It is worth outlining that every individual optical flow occupies its own S-BVT VCSEL and Co-Rx at the ingress and egress nodes, as well as allocates a dedicated optical spectrum over the traversed path's links. Herein the occupied optical spectrum by an optical flow is referred to as Frequency Slot (FS).

The physical impairments accumulated over the optical signal while travelling from the source to the destination may end up with a received net data rate lower than  $r^{VCSEL}$ . To model this, in [5] it was defined three different received data rates for the same VCSEL associated to the so-called *operational modes* (OMs): *high*, *medium*, and *low*. Specifically, each OM determines different supported data rates depending on the maximum end-to-end path distance (km) and number of hops. Figure 1 lists for each defined VCSEL OM the data rate at the receiver as long as the maximum values for the route distance (i.e., aggregating the fiber length of all the traversed links) and the number of traversed optical switches (i.e., hops) are not exceeded.

| VCSEL Mode (OM) | $r$ (Gb/s) | Max. Distance (km); #Hops |
|-----------------|------------|---------------------------|
| High            | 50         | 30; 5                     |
| Medium          | 40         | 75; 9                     |
| Low             | 25         | 150; 15                   |

**Fig. 1.** Defined VCSEL Operational Modes (OMs) describing the data rate (Gb/s), maximum path distance (km) and number of hops.

In [5], the authors presented and evaluated a Routing and Spectrum Assignment (RSA) algorithm which dynamically serves connection requests demanding different bandwidth (i.e., data rate) over the PASSION metro network solution (i.e., using the above HL nodes and the VCSELs' OMs). This RSA algorithm builds upon a modified K shortest path (K-SP) referred to as co-routed optical flows (RSA-CR). For a given *req*, the RSA-CR algorithm computes the necessary optical flows to fulfil the *req*'s bandwidth (i.e.,  $b$ ) considering the most convenient VCSEL's OM. For the sake of clarification, the most convenient OM means to foster selecting those paths enabling the VCSELs at the ingress nodes attaining the highest net data rates at the receiver. All the resulting optical flows from the RSA output are set up along the same spatial path (i.e., nodes and links) but occupying different FSs. The latter entails that each optical flow also occupies different S-BVT VCSELs and CO-Rxs. Bearing this in mind, herein we extend [5] proposing an RSA-CR algorithm variant. The new RSA algorithm leverages the *inverse multiplexing* capability within flexigrid optical networks [6]. That is, *req*'s optical flows can be routed over different spatial paths. The algorithm is referred to as RSA inverse multiplexed (RSA-IM) optical flows.

Both algorithms (RSA-CR and RSA-IM) are experimentally evaluated within the CTTC ADRENALINE testbed considering dynamic connection request with different bandwidth needs. The obtained results and comparison are realized using three performance metrics: the *blocked bandwidth ratio* (BBR), the average number of occupied S-BVTs VCSELs and CO-Rxs, and the average connection establishment (setup) time.

## 2 Targeted Optical Metro Network

Fig. 2 depicts a candidate PASSION SDN-controlled flexi-grid optical metro network topology. All the *reqs* arrive to the SDN controller from a Connection Request Application requests (via a RESTful API). The SDN controller is then in charge to compute the path and select the resources triggering the RSA algorithms. If the RSA succeeds, the selected resources are configured via dedicated control interfaces (RESTful API) as detailed in [5].

In the following, a description of the metro optical infrastructure involving the S-BVT and HL optical switches is provided. Next, it is also reported the key functions and operations handled by the SDN controller to attain the automatic configuration of the underlying transport network and devices when setting up connections.

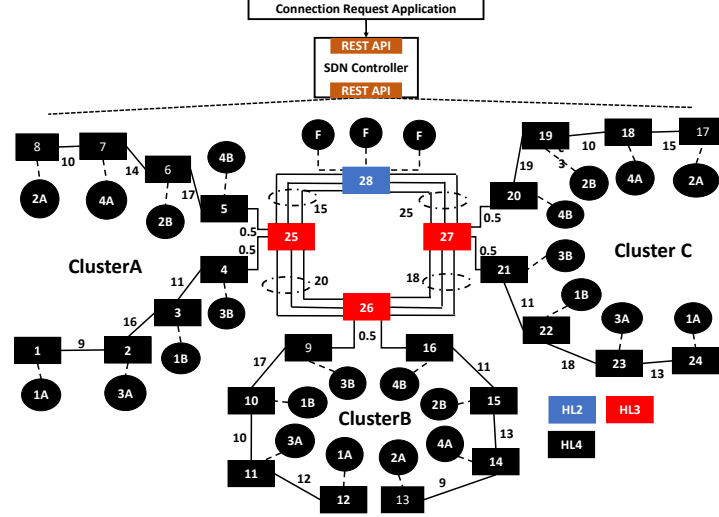


Fig. 2. Targeted SDN-controlled Optical Metro Network.

## 2.1 Network Topology, S-BVTs and Optical Switches Features

The metro network topology is a star-ring infrastructure with three *clusters* (i.e., A, B and C). A cluster is made up of a pair of linear networks connected to a 4-node ring topology. Each linear network constitutes a *branch*. All the nodes are associated to a specific HL type as mentioned above. HL4 nodes (black squares in Fig. 2) deal with the access traffic aggregation. Additionally, HL4 node are equipped with an S-BVT. formed by a single Module with 20 VCSELs. Thus, HL4 S-BVTs can provide a maximum capacity of  $20 \times r^{VCSEL}$ , i.e., 1 Tb/s (if all the VCSELs operate at the *high OM*). Analogously, HL4 S-BVT Rxs are deployed with 20 CO-Rxs. Each S-BVT VCSEL is bound to a specific wavelength within the 191.900 - 195.875 THz spectral range. As a result, to support in a *cluster* all the frequencies in the targeted range, it is needed that each cluster *branch* uses 4 HL4 nodes. The wavelengths in the 4 S-BVTs for each individual *branch* are separated 50 GHz. The considered wavelength planning is detailed in Fig. 3. Clusters' S-BVTs are named as 1A, 1B, 2A, ..., 4B. In the HL4 cluster (formed by 2 branches) the resulting wavelengths among all the S-BVTs' VCSELs are spectrally separated 25 GHz. HL4 optical switches are constructed upon Array Wavelength Grating (AWG) filter of 50 GHz.

The HL3 nodes form the ring topology being shown in Fig. 2 as red squares. These optical switches enable the interconnection between HL4 and HL2/1 nodes and are built on 25 GHz filters using Wavelength Selective Switches. HL3 nodes exclusively support the optical aggregation and bypass without originating/terminating optical flows, i.e. HL3 nodes do not have S-BVTs.

Finally, the HL2/1 node (blue squares in Fig. 2) are also made up of 25 GHz WSSs and interface the core network segment with 3 fully equipped S-BVTs. As detailed in Fig. 3, these fully equipped S-BVTs have 160 VCSELs and 160 CO-Rxs. That is, all

the targeted spectral range is covered by one of these S-BVTs offering a transmission capacity of up to  $160 \times r^{VCSEL}$ , i.e., 8 Tb/s.

The modularity of the S-BVT designed within the PASSION project is attained thanks to a hierarchical architectural approach made up of a 3-tuple Module/subModule/VCSELs. Detailed description of the PASSION S-BVT can be found in [4]. A Module represents an *atomic* S-BVT element based on a photonic integrated chip. Taking advantage of the so-called modularity capability, different Modules (up to 4) could be arranged to provide S-BVT offering larger transport capacity depending on the bandwidth needs. Every Module integrates 4 subModules. A subModule is formed by 10 VCSELs each. Consequently, a S-BVT made up of a single Module is able to provide at the transmitter a data rate of up to: 4 (subModules)  $\times$  10 VCSELs  $\times r^{VCSEL}$ , i.e., 2 Tb/s. In the HL2/1 S-BVTs, observe that the S-BVTs have 4 Modules which offers a maximum transmission capacity of 8 Tb/s. At the S-BVT Receiver (Rx), CO-Rxs with tunable local oscillators are used.

| S-BVT    | #VCSELs<br>& CO-Rxs | Supported Frequencies (THz)             |
|----------|---------------------|-----------------------------------------|
| 1A       | 20                  | 191.900, 192.100, 192.300, ..., 195.700 |
| 1B       | 20                  | 192.000, 192.200, 192.400, ..., 195.800 |
| 2A       | 20                  | 191.925, 192.125, 192.325, ..., 195.725 |
| 2B       | 20                  | 192.025, 192.225, 192.425, ..., 195.825 |
| 3A       | 20                  | 191.950, 192.150, 193.350, ..., 195.750 |
| 3B       | 20                  | 192.050, 192.250, 192.450, ..., 195.850 |
| 4A       | 20                  | 191.975, 192.175, 192.375, ..., 195.775 |
| 4B       | 20                  | 192.075, 192.275, 192.475, ..., 195.875 |
| Full (F) | 160                 | 191.900, 191.925, 191.950, ..., 195.875 |

**Fig. 3.** S-BVT with number of deployed VCSELs and CO-Rx and the supported wavelengths.

## 2.2 SDN Network Programmability

In [7], it is detailed the design and validation of the SDN controller to handle the programmability of the targeted metro transport network and devices (i.e., S-BVTs and HL optical switches). Such an SDN controller architecture tackles:

- the RESTful API to receive connection requests (*req*),
- the RESTful APIs to communicate with the network elements and devices agents enabling the (de-)allocation of the optical resources.
- the functions supporting the operations of the SDN controller.

The SDN controller functions enable a) handling the optical connection lifecycle (i.e., establishment and removal); b) collecting updated resource information from the network element and agents; and c) executing the RSA algorithm to seek for a feasible path and optical resources fulfilling the *req* demands as well as attaining an efficient use of the overall network resources. The following focuses on describing the devised RSA-CR and RSA-IM algorithms upon processing a new *req*.

### 3 Routing and Spectrum Assignment (RSA) Algorithms

Each received connection request (i.e., *req*) specifies the source and destination endpoints (i.e., *s* and *d*, respectively) along with the required bandwidth (i.e., *b*). Regardless of the executed RSA algorithm (RSA-CR or RSA-IM), the inputs are: i) the network topology (i.e., node connectivity, link distance, etc.) and the available optical spectrum over each link; ii) the available S-BVT VCSEL and Co-Rx resources at *s* and *d* endpoints, respectively. A successful RSA computation provides the following output: i) the nodes and links to be traversed by each optical flow; ii) the selected S-BVT VCSELs at *s*; iii) the CO-Rxs (with their tuned local oscillators) at *d*; iv) the optical spectrum (i.e., FS) to be allocated for each required optical flow.

#### 3.1 RSA Co-Routed (RSA-CR) Optical Flows

This algorithm was proposed and evaluated in [5]. It is based on a modified K shortest path (K-SP) mechanism. The aim of the RSA-CR algorithm is to serve a *req* satisfying the spectral constraints and achieving an efficient use of all the network resources. The RSA-CR returns the first  $k^{\text{th}}$  SP that accommodates the set of optical flows for a *req* over the same nodes and links. To this end, the RSA-CR algorithm operates in a two-step approach. In step 1, it is computed the K-SPs between *req*'s *s* and *d* nodes. Then, in Step 2, for each computed  $k^{\text{th}}$  path, starting from the highest VCSEL OM (see Table 1), it is first checked whether that path fulfills the targeted OM's maximum distance and number of hops. If yes, then it is determined the number of required S-BVT VCSELs and optical flows to satisfy the *req*'s *b*, as well as the optical spectrum assignment for the optical flows. For the latter, observe that it is needed to consider: i) the available VCSELs optical carriers; ii) the unused optical spectrum through all the path links; and iii) optical flows are subject to the spectrum continuity and contiguity constraints. If either the OM's maximum distance or number of hops is not satisfied by the considered path, a lower VCSEL OM is explored and the spectrum assignment mechanism is checked. The RSA fails when no sufficient S-BVT resources are available at the endpoints or the spectrum constraints for the required optical flows cannot be fulfilled for any of the K-SPs.

Fig. 4 (left) shows an example of the RSA-CR algorithm. Let us assume that a *req* of 100 Gb/s between nodes 9 and 28 arrives. Moreover, we consider that the high OM is feasible. This means that a path connecting node 9 and 28 (e.g., 9-26-25-28) does not exceed the maximum path distance and number hops determined by the *high* OM. Thus, the S-BVT VCSEL at the node 9 operates at the maximum data rate ( $r^{\text{VCSEL}}$ ), i.e. 50 Gb/s. To fulfill the *req* bandwidth demand, two VCSELs need to be allocated at node 9 and two CO-Rxs at node 28. This does entail on setting up two individual optical flows referred to as X and Y. The flow X occupies the node 9 S-BVT VCSEL at the wavelength 192.050 THz; the flow Y allocates the VCSEL at the wavelength 192.250 THz. The VCSEL's wavelengths for both X and Y flows identify the central frequency (*n*) of the respective FSs. The FS slot width (*m*) depends on the traversed HL optical switch and their filtering features. At node 9 (i.e., HL4), the FS of the flow X occupies  $n = -168$  (ITU-T channel for 192.050 THz) and  $m = 4$  (slot width of 50 GHz). For the

flow Y, at the same node, the FS is  $n = -136$  and  $m = 4$ . Nevertheless, at HL3 nodes (i.e., 26 and 25) and HL2/1 node (28) with 25GHz WSS filters, the FS for the flow X uses  $n = -166$  and  $m = 2$ . Likewise, for the flow Y, the FS in those nodes is  $n = -134$  and  $m = 2$ . Observe that according to the traversed HL node, the FS  $n$  and  $m$  may vary for a given flow. However, the optical spectrum transporting the effective data is invariant.

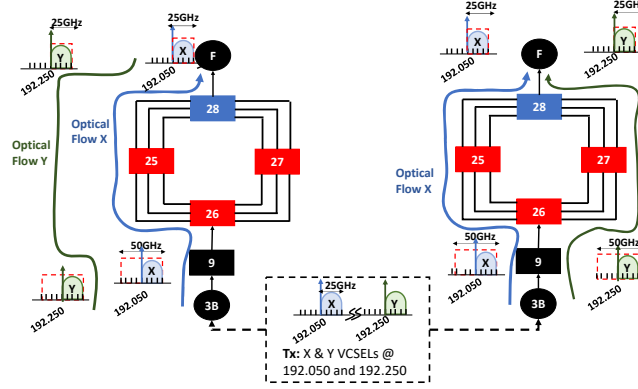


Fig. 4. Example of RSA-CR (*left*) and RSA-IM (*right*).

### 3.2 RSA Inverse Multiplexing (RSA-IM) Optical Flows

The RSA-IM algorithm is similar to the RSA-CR mechanism but rather than enforcing that all the optical flows are routed over the same spatial path, this is relaxed enabling to accommodate the optical flows over different nodes and links between  $s$  and  $d$  nodes. As in the RSA-CR algorithm, first it is computed the K-SPs. Then, starting from the highest VCSEL's OM, it is determined the number of VCSELs and optical flows to be allocated. If for the considered VCSEL's OM, no path fulfills the OM's maximum distance and number of hops are discarded, a lower VCSEL's OM is explored. Otherwise, it is created a subset of the K-SPs forming the pool of candidate paths satisfying the under-considered VCSEL's OM requirements. This candidate set of paths is then explored to accommodate the required optical flows. That is, for every optical flow, the algorithm iterates over the resulting candidate paths seeking for a feasible FS (i.e., subject to the available S-BVT VCSEL and the unused optical spectrum on every path). If the candidate paths cannot accommodate all the optical flows for  $req$ , the connection is blocked.

Fig. 4 (right) shows the example for the RSA-IM algorithm. As in the previous example, a  $req$  of 100 Gb/s between nodes 9 and 28 needs to be set up; assuming high VCSEL's OM, X and Y optical flows are set up allocating the VCSEL wavelengths at 192.050 THz and 192.250 THz, respectively. X and Y flows are routed over different spatial paths, namely, X flow traverses the path formed by the node sequence 9-26-25-28, whilst Y flow is accommodated over the path 9-26-27-28. The aim of the RSA-IM algorithm when compared to the RSA-CR strategy is to favor fulfilling the spectrum

contiguity and continuity constraint mostly within the subnetwork formed by the HL3 all-optical switches.

## 4 Experimental Evaluation

The performance evaluation of both RSA-CR and RSA-IM algorithms under dynamic connection requests is carried out at the CTTC ADRENALINE control plane [8]. The network topology shown in Fig. 2 is deployed over 28 Linux-based servers. Each server hosts an HLx node agent to emulate the optical flow establishment. Those servers hosting the HL4 agents (i.e., nodes 1 to 24) also provide the S-BVT device agents. The server for the node 28 agent co-locates three fully equipped S-BVT agents.

The connection requests are generated using Poisson process with an average inter-arrival time of 5 s. The duration of each connection (i.e., holding time, HT) is exponentially modeled. The HT mean is varied to attain multiple traffic loads. For each *req*, the *s* and *d* are randomly chosen to request a connection between HL4 nodes and (HL2/1), and viceversa. The *req*'s *b* is uniformly distributed as multiple of 50 Gb/s up to 200 Gb/s. 10k connection requests are generate for each data point. Links are formed by bidirectional optical fibers supporting 644 NCFs (spaced 6.25 GHz) covering the 191.900 - 195.875 THz spectrum range. The length of every link is labelled on each edge as depicted in Fig. 2. This information is needed to the adopted RSA algorithm to assess and select the most efficient VCSEL OM for a computed path. For different HT values, it is compared the performance attained when adopting either RSA-CR or RSA-IM algorithms. This comparison is realized also considering different K-SP values: 1, 3, 6 and 9. The performance metrics for such a RSA algorithm comparison are: i) the BBR; ii) the average number of used S-BVTs VCSELs and CO-Rxs; and iii) the average connection setup time. The BBR is defined as the attained ratio between the blocked bandwidth (accounting for the failed connections) and the total requested bandwidth. Thus, the lower the BBR, the better an RSA performs.

Fig. 5 depicts the obtained BBR performance by both RSA-CR (left) and RSA-IM (right) for  $K = 1, 3, 6$  and  $9$  with respect to different HT. As expected for both RSA algorithms, as HT grows the BBR performance is worsened. Since more optical flows occupying resources (i.e., S-BVT VCSELs and CO-Rxs, links' NCFs) co-exist, this does complicate the RSA algorithm to find a feasible path and FS for the *req*'s optical flows. There are two RSA failing causes: i) not enough unused S-BVT VCSELs or CO-Rx at either *s* or *d*; ii) unable to ensure the spectrum constraints for all the *req*'s optical flows. For the second failure reason, since the S-BVT Tx VCSELs are associated to a given wavelength, this significantly narrows the set of feasible FSs when setting up an optical flow. That is, the S-BVT VCSELs not used at the *s* restricts the usable optical spectrum for the optical flows' FSs. Consequently, if one increases the K-SP number, larger spatial paths can be considered by the RSA algorithm. This leads to favor finding a  $k^{\text{th}}$  path that supports a feasible FS fulfilling the spectrum constraints for each flow. Thereby, as  $K$  increases, the BBR enhances specially with respect to  $K=1$ . This behavior is seen in both RSA algorithms. However, the improvement becomes less significant when passing from  $K=3$  to  $6$  and  $9$ . The reason behind this is that increasing  $K$  may



result on considering longer paths (in terms of hops and distance). Such long paths make the RSA algorithm to use the lowest OM for the S-BVT VCSELS. As a result, the number of required optical flows for a *req* is increased which yields on not only uses more S-BVT resources but also notably complicates satisfying the spectrum constraints for each optical flow.

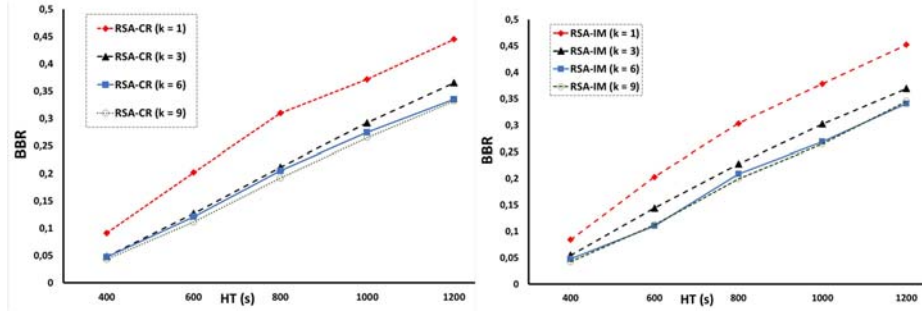


**Fig. 5.** BBR vs HT ( $K = 1, 3, 6$  and  $9$ ); RSA-CR (left), RSA-IM (right).

Fig.6 (a) compares the BBR performance attained by both RSA-CR and RSA-IM algorithms for both  $K=1$  and  $9$ . We observe that both RSA algorithms perform similarly. Thus, the capability of the RSA-IM algorithm to route *req*'s optical flows over different paths with the purpose to better fulfil the spectrum constraints does not bring an improvement. The reason behind this is that the considered network infrastructure only enables route flexibility within the transit ring topology formed by nodes 25, 26, 27 and 28. This considerably narrows the route diversity that could be attained by the RSA-IM algorithm. In this regard, an interesting follow-up of this work is to explore how the network topology and node connectivity impacts on the performance of both RSA algorithms.

Fig.6 (b) provides the average used S-BVT VCSELS and CO-Rxs for both different HT and  $K$  values attained by the considered RSA algorithms. As aforementioned, a higher  $K$  value leads to enhance the BBR performance, i.e. larger *reqs* can be successfully accommodated. Consequently, this does increase the number of average used S-BVT VCSELS and CO-Rxs. As an example, for  $K=1$  adopting the RSA-CR algorithm, the average used S-BVT VCSELS and CO-Rx are 10,2 for  $HT=400s$ . For a higher  $K$  (i.e., 9) and the same  $HT=400s$ , such an average utilization grows to 10,6. Moreover, as the traffic load becomes higher ( $HT=1200s$ ), the average used S-BVT VCSELS and CO-Rxs do increase more significantly. Specifically, for the RSA-CR algorithm, the average utilization of the S-BVTs at  $HT=1200s$  ranges 16,1 – 16,2 at  $K=1$ ; whilst at  $K=9$ , this average utilization metric reaches 19,2. Recall that as shown in Table 2, at the HL4 nodes the number of S-BVT VCSELS and CO-Rxs is 20. Thus, at  $K=9$  and  $HT=1200s$  most of the S-BVT resources are averagely occupied. Similar trend is accomplished when the RSA-IM algorithm is applied. In general, increasing the  $K$  value, allows the algorithm exploring larger number of candidate paths. Thereby, this provides higher spatial path flexibility which eases satisfying feasible *req*'s optical flows fulfilling spectrum constraints. As a result, more concurrent connections co-exist within the network leading to increase the average used of S-BVT VCSEL and CO-Rx devices.

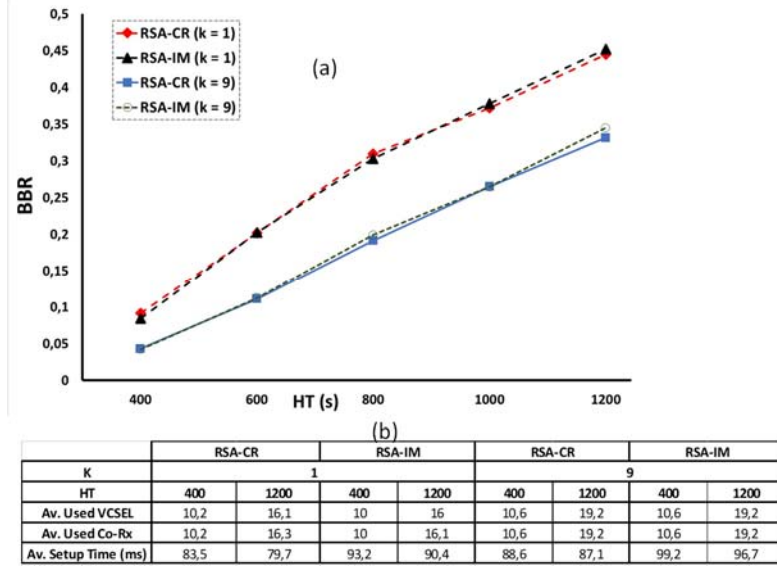


**Fig. 6.** (a) BBR performance comparing RSA-CR and RSA-IM ( $K=1$  and  $9$ ); (b) average used S-BVT VCSEL and Co-Rx and Average Setup Time for both RSA-CR and RSA-IM

The above improvement in both BBR performance and S-BVT resource utilization when increasing the  $K$  value (in RSA-CR and RSA-IM) are attained at the expenses of slightly increasing the average setup time as seen in Fig.4 (b). That is, the larger is the number of  $K$  pre-computed spatial paths, the higher the RSA computation time is. Additionally, in the RSA-IM algorithm, we observe that regardless of the HT, the average setup time is larger than those results attained by the RSA-CR algorithm. The reason of this is that in the RSA-IM algorithm for each *req*'s optical flow, all the pre-computed  $K$ -SPs are checked. This, however, does not happen in the RSA-CR algorithm where for all *req*'s optical flow only a single  $K$ -SP is checked for each iteration. Consequently, the RSA-IM algorithm tends to seek over more candidate  $K$ -SPs when computing each *req* resulting on a larger computational time, and in turn, higher average setup time.

## 5 Conclusions

The deployment of 5G technology fulfilling their requirements in terms of transport capacity, latency, etc. impacts significantly in the design of the upcoming metro network infrastructures. It is well-accepted that photonic technologies result an appealing enabler to deploy high-capacity, low-cost, and energy efficient metro networks. The EC-H2020 PASSION project investigates solutions on these metro network challenges via: i) SDN configurable and modular S-BVT devices leveraging VCSEL technologies; and ii) hierarchical flexi-grid optical networks. In [5] the RSA-CR algorithm was presented and evaluated to dynamically accommodate heterogenous data rate connections within the targeted metro network. Herein, this algorithm is extended through

proposing the RSA-IM algorithm. The RSA-IM aims at relaxing the necessity of routing all optical flows of a given connection over the same spatial path. This may lead to better satisfy the optical flows' spectrum constraints. Both RSA algorithms are compared upon dynamic connection arrival varying the K value of the K-SP computation. We observe that both RSA algorithm attains similarly on the BBR metric. Thus, the BBR enhancement envisaged by the RSA-IM algorithm thanks to a better flexibility to route *req*'s optical flows over diverse spatial paths is not reflected. This may be caused by the considered metro network ring-star topology (showed in Fig.2). One may realize that this topology lacks having significant path diversities to be exploited by the RSA-IM. Next studies will concentrate on assessing both algorithms over metro network topologies with higher nodal degree and network connectivity.

## Acknowledgements

The research leading to these results has received funding from the EUH2020 PASSION Project (780326) and by Spanish MICINN AURORAS (RTI2018-099178-B-I00) project and Spanish Thematic Network Go2Edge (RED2018-102585-T).

## References

1. CISCO White Paper, "Cisco Visual Networking Index: Forecast and Trends, 2017 - 2022 White Paper," Feb. 2019.
2. M. Svaluto Moreolo, J. M. Fabrega, L. Nadal, R. Martínez and R. Casellas, "Synergy of Photonic Technologies and Software-Defined Networking in the Hyperconnectivity Era," IEEE J. of Lightwave Tech., vol. 37, no. 16, Aug. 2019.
3. EC H2020 PASSION Project, <http://www.passion-project.eu/wpcontent/uploads/2018/01/PASSION-Project-Fact-Sheet.pdf>
4. P. Paroli, A. Gatto and P. Boffi, "Long Wavelength VCSELs Exploitation for Low-Cost and Low-Power Consumption Metro and Access Network," in Proc. of 20th International Conference on Transparent Optical Networks (ICTON), July 2018.
5. R. Martínez, et. al., "Experimental Evaluation of an On-line RSA Algorithm for SDN-Controlled Optical Metro Networks with VCSEL-based S-BVTs" in Proc. of IFIP/IEEE Optical Network Design and Modelling (ONDM), May 2020
6. M. Jinno, H. Takara, B. Kozicki, Y. Tsukishima, Y. Sone, and S. Matsuoka, "Spectrum-efficient and Scalable Elastic Optical Path Network: Architecture, Benefits, and Enabling Technologies", IEEE Communications Magazine, Nov. 2009.
7. R. Martínez, et. al., "Design and Deployment of an SDN programmable Optical Metro Network with VCSEL-based S-BVTs" in Proc. of International Conference on Transparent Optical Networks (ICTON 2020), July 2020.
8. R. Muñoz, et. al., "The ADRENALINE Testbed: An SDN/NFV Packet/Optical Transport Network and Edge/Core Cloud Platform for End-to-End 5G and IoT Services," In Proc., of European Conference on Networks and Communications (EuCNC), June 2017